The Cryosphere Discuss., 7, 1215–1242, 2013
www.the-cryosphere-discuss.net/7/1215/2013/
doi:10.5194/tcd-7-1215-2013

The Cryosphere Discussions
Open Access

Waveform analysis of airborne synthetic aperture radar altimeter over Arctic sea ice

M. Zygmuntowska[1], K. Khvorostovsky[1], V. Helm[2], and S. Sandven[1]

[1]Nansen Environmental and Remote Sensing Center, Bergen, Norway
[2]Alfred Wegener Institute, Bremerhaven, Germany

Received: 4 February 2013 – Accepted: 5 March 2013 – Published: 22 March 2013

Correspondence to: M. Zygmuntowska (marta.zygmuntowska@nersc.no)

Published by Copernicus Publications on behalf of the European Geosciences Union.

Abstract

Sea ice thickness is one of the most sensitive variables in the Arctic climate system. In order to quantify changes in sea ice thickness, CryoSat was launched in 2010 carrying a Ku-band Radar Altimeter (SIRAL) designed to measure sea ice freeboard with a few centimeters accuracy. The instrument uses the synthetic aperture radar technique providing signals with a resolution of about 300 m along track. In this study, airborne Ku-band radar altimeter data over different sea ice types has been analyzed. A set of parameters has been defined to characterize the difference in strength and width of the returned power waveforms. With a Bayesian based method it is possible to classify about 80 % of the waveforms by three parameters: maximum of the returned power echo, the trailing edge width and pulse peakiness. Furthermore, the radar power echo maximum can be used to minimize the rate of false detection of leads compared to the widely used Pulse Peakiness parameter. The possibility to distinguish between different ice types and open water allows to improve the freeboard retrieval and the conversion into sea ice thickness where surface type dependent values for the sea ice density and snow load can be used.

1 Introduction

While arctic sea ice extent and its changes have been studied widely in the last decades (Kwok, 2002; Comiso et al., 2007; Stroeve et al., 2012) sea ice thickness and its decrease remain one of the least observed variables in the arctic climate system (Laxon et al., 2003; Maslanik et al., 2007; Giles et al., 2008; Kwok and Rothrock, 2009). Ice thickness data are highly limited and only available from sparse campaigns with upward looking sonars on submarines and moorings (Rothrock et al., 1999, 2008) or helicopter surveys using electro-magnetic induction (Haas et al., 1997, 2010, 2011; Hendricks et al., 2011). Satellite laser and radar altimeters have provided large-scale coverage of ice thickness data in the Arctic, but their capabilities are limited to certain

TCD
7, 1215–1242, 2013

periods and regions. ICESat has been only operated for two six-week periods per year from 2003 to 2008 (Kwok et al., 2004; Kwok and Untersteiner, 2011), while conventional altimeters on-board ERS-1/2 and ENVISAT have relatively coarse resolution and cover the polar regions only up to 81.5° N (Laxon et al., 2003). In 2010 CryoSat-2 was launched with the main objective to study changes of the cryosphere (Drinkwater et al., 2004). CryoSat's payload instrument is the SAR/Interferometric Radar Altimeter (SIRAL) which uses the synthetic aperture radar technique to enhance the resolution along track. When operating in SAR mode over sea ice CryoSat has a footprint of about 270 m × 1000 m, which is a significant improvement compared to the previous ERS and ENVISAT altimeters.

Since the 1980s radar altimeter signals from sea ice have been analyzed in many studies (Dwyer and Godin, 1980; Onstott et al., 1987). Using data from the GEOS-3 satellite, Dwyer and Godin (1980) published the first analysis of radar altimeter waveform signal over sea ice. They found altimeter echo waveforms over smooth sea ice to rise to a higher value than over the rough open ocean. Drinkwater (1991) and Ulander (1987) found correlations between radar backscatter in SAR images and radar altimeter echo strength and width. Fedor et al. (1989) observed a reduction of the signal response from flat to ridged sea ice. The strongest return signal comes from leads with calm open water or thin ice, producing specular echo power waveforms (Fetterer, 1992). Encouraged by these findings the possibility for sea ice classification based on radar altimeter data alone has been discussed in several studies (Chase and Holyer, 1990; Drinkwater, 1991; Laxon, 1994a). Even though the results were promising the methods have not been developed any further. The current ENVISAT algorithm for example distinguishes only betwenn leads and ice floes, whereas open water areas are masked out by use of passive microwave data (Laxon et al., 2003; Giles et al., 2008; Ridout et al., 2012). Leads are identified most commonly by the pulse peakiness parameter – a measure of the ratio of signal maximum and accumulated power (Peacock and Laxon, 2004; Giles et al., 2007). Sea ice thickness is retrieved using prescribed values for ice density and climatological snow depth (Warren et al., 1999).

TCD
7, 1215–1242, 2013

All the assumptions used in this algorithm are based on conventional altimeters where the waveform is essentially a step function. Once the power has reached the maximum it remains there for many delay intervals as the area contributing to the power echo is constant over time (Brown, 1977). For synthetic aperture radar altimeters the signal decays more rapid after the peak as the area contributing to the response signal decreases with square root of time (Raney, 1998). The different sampling technique and the resulting different echo shape suggests that a classification of different sea ice types only using waveform data from synthetic aperture radar altimeters may be possible.

In this study attempts are made to distinguish between first year ice and multi year ice based on the shape of the radar echo waveform alone. The data used in the study were obtained by an airborne synthetic aperture radar altimeter during pre-launch calibration and validation campaigns for CryoSat-2. Different parameters to describe the returned signal and techniques for classification have been explored. The paper contains the following sections: in Sect. 2 the instruments, datasets, campaigns, and parametrization of waveforms are described (2.2) as well as the classification methods (2.3). The distribution of each parameter for different surface types and the resulting classification rates are given in Sect. 3. In Sect. 4 the results are compared to previous results from conventional altimeters and perspectives for further applications are discussed.

2 Data and methods

2.1 Instrument and data campaign

To examine the possibilities of surface classification based on radar altimeter data, measurements from ESAs CryoSat calibration and validation experiments CalVal 2007 and CalVal 2008 have been used. Both airborne operations were coordinated by the National Space Institute, Danish Technical University (DTU Space) and the Alfred Wegener Institute (AWI). In 2007 the campaign was carried out from 15 to 25 April while in

TCD
7, 1215–1242, 2013

2008 it lasted from 15 April until the 8 May. In this study mainly data from the Airborne Synthetic Aperture and Interferometric Radar Altimeter System (ASIRAS) are used. The instrument is operating at a center frequency of 13.5 GhHz (Ku-band) and features along track resolution enhancement by using the synthetic aperture radar technique like its satellite counterpart SIRAL on-board CryoSat. ASIRAS operates with an antenna beam pattern of 10 degrees along track and 2.5 degrees across track which results in a resolution of 3 m along track. The return echo power for each data point is recorded with a vertical resolution of approximately 0.095 m and sampled in a 24 m range window, corresponding to 256 bins. Since CryoSat-2 is primarily designed to measure trends in the perennial sea ice, the main validation campaigns took place north of Greenland, which is known to be an area mostly covered by this type of ice. Single flights have also been performed in the Baffin bay and around the Svalbard archipelago. Therefore we were able to analyze the returned signal over different surfaces such as leads, first year ice (FYI) and multi year ice (MYI) (see Table 1). Besides the area of acquisition the surface types have been identified on contemporary Envisat ASAR images (see Fig. 2). In some of the areas, as in the first year and multi year ice cases north of Alert, aircraft validation has been performed during the campaign and detailed in-situ measurements were also available. The area has also been overflown by an airborne electromagnetic-induction device (EM-Bird) to measure ice thickness. Additionally, data from downward looking optical cameras onboard the airplanes were available. The combination of these datasets gives a precise knowledge of the ice conditions and allows for a detailed study of the waveform signal over different surface regimes. More information about the campaigns can be found in the technical reports (Helm and Steinhage, 2008; Hvidegaard et al., 2009; Cullen and Davidson, 2009). An overview of the location of the analyzed cases is given in Fig. 1. Table 1 provides an overview of the cases for each surface type with the number of available waveforms, additional data sets as well as the acronym which will be used for each case.

TCD
7, 1215–1242, 2013

2.2 Parametrization of waveform shape

The return signal from the radar altimeter is sampled in a range window of 256 bins, each with a size of about 0.095 m. The signal is usually referred to as power echo waveform or simply waveform. To be able to describe the shape of the waveform quantitatively and account for the differences in strength and width of the signal the following parameters have been used (see Fig. 3):

- *Maximum (Max)* value of the power echo.
- *Pulse Peakiness (PP)* is the ratio of the maximum power to the accumulated echo power (first defined by Laxon, 1994b).

$$\mathrm{PP} = \frac{\max(\mathrm{power})}{\sum_{i=1}^{256} \mathrm{power}(i)} \quad (1)$$

- *Leading Edge Width (LeW)* is obtained by fitting a Gaussian curve to the leading edge (starting at the bin containing an echo power larger than 1 % of the power maximum and ending two bins after the bin with the maximum value). The distance between 1 % and 99 % of maximum power echo is defined as the Leading Edge Width (e.g. Legresy et al., 2005).
- *Trailing Edge Width (TeW)* is obtained by fitting an exponential decay function to the trailing edge starting with the bin containing the maximum power. The Trailing Edge Width is the distance between the 99 % and 1 % of the power maximum (e.g. Legresy et al., 2005).
- *Trailing Edge Slope (TeS)* is the decay factor for the exponential fit (e.g. Legresy et al., 2005).

TCD
7, 1215–1242, 2013

2.3 Classification parameters and methods

To evaluate which parameters are most distinct for each surface type and therefore suitable to distinguish between surface classes the Kolmogorov-Smirnov test (KS-test) has been applied. In statistics, the KS-test makes it possible to determine if two datasets differ significantly by quantifying the distance between the empirical cumulative distribution functions of two samples. No assumption about the distribution of the two data samples is made but the test is sensitive to differences in location and shape of the distribution functions.

After analyzing the probability distributions and finding the parameters that are most suitable for classification, two different classification methods have been explored: (1) rule based threshold method and (2) Bayesian classifier. The threshold method is the one most commonly applied to detect leads within sea ice. The Bayesian classifier is a simple and robust classification method based on supervised learning that formulates the classification problem in probabilistic terms.

2.3.1 Rule based threshold

By analyzing the distribution functions for different surface classes and waveform parameters it seems straight forward to base a classification on simple thresholds between the classes. This is a widely used method to identify leads and usually the Pulse Peakiness parameter or the Maximum are used (Peacock and Laxon, 2004; Giles et al., 2007; Röhrs and Kaleschke, 2012). We selected an equal number of waveforms from each surface class and set the threshold by maximizing the number of correct classified waveforms from this selection. To minimize the number of false detection a margin has been set around the threshold. The size of the margin equals approximately 2 % of the range of each parameter. Waveforms with classification parameters within this margin are labeled as not classified. The advantages of this rule based threshold method are that no assumption on the distribution is made and it is very easy to implement after setting the threshold.

TCD
7, 1215–1242, 2013

2.3.2 Bayesian classifier

For the classification with the Bayesian approach our dataset has been divided into two different parts: a learning data set with 40 % of all available waveforms and a testing set with 60 %. The Bayesian classifier is based on Bayes theorem (Bayes and Price, 1763) which formulates the classification problem in probabilistic terms: based on the probabilities of each surface class and probabilities of the waveform parameters for each class a probability calculation is used to make a classification decision. Parameters are here ,e.g. Pulse Peakiness, Trailing Edge Width, Max and the classes are the two ice types and leads. In our study we used Gaussian kernel density estimates to model the parameter densities for each class. It is assumed that parameters are conditionally independent and their class distributions are calculated independently. To reduce the number of wrong classification we added the requirement that the probability belonging to one class has to be higher than 70 %. Otherwise waveforms were labeled as not classified.

3 Results

3.1 Typical waveform

As a first qualitative analysis we show mean waveforms for different surface types in Fig. 4. To account for the difference in surface elevation all waveforms have been moved such as their maximum values are located in the same sampling bin. The mean maximum echo power resulting from reflection over leads is more than 8 times higher than from those coming from sea ice; and even 4 times higher than the mean maximum coming from flat first year ice (Fig. 4a). The difference in the maximum from the waveforms coming from first year ice and multi year ice is less distinct. In Fig. 4b normalized waveforms are shown to visualize the difference in the width of the power echo.

TCD
7, 1215–1242, 2013

Based on the visual analysis of the waveforms there is clear difference in the decay after the peak – multi year ice having a lower decay rate and a wider trailing edge than first year ice and leads. Reflection over flat FYI (black line) does however not result in a wider signal than over leads.

3.2 Distribution of the parameters

The cumulative probability distributions for each parameter for the nine analyzed cases are shown in Fig. 5. As the term first year ice is very wide – ranging from undeformed thin ice to ice which has undergone a high rate of deformation – the spread of the distributions coming from this surface class is quite large for all parameters.

In particular the spread for the FYI distributions of the power maximum is very wide and reaches both extremes: distributions are observed with much smaller and higher values than coming from the MYI cases. The two cases of sea ice with the largest signal are flat new ice (FYI3) and fast ice (FYI1). In all cases however the distributions differ substantially from those obtained over leads (L1 and L2).

For the Pulse Peakiness the distributions of the cases of MYI and leads closely resemble each other within these classes. The distributions for FYI however differ again largely from case to case. The PP resulting from the power echo of flat thin ice (FYI3) are almost as high as those resulting from the waveform of leads, while all other cases show clearly smaller PP values. Reflection from FYI results on average in higher PP values than from MYI, but the cumulative probability distribution from FYI and MYI overlap to a high extend.

The distributions of the parameters related to the leading and trailing edge, hence the TeW, LeW and TeS, look much alike: narrow and similar distributions for the two evaluated cases of leads, a wide spread in the distributions for FYI, and wide distributions with long tails for the MYI.

However, even though we found a large spread in the distributions for each class and sometimes large overlaps between single cases from different classes, the averaged

TCD
7, 1215–1242, 2013

distributions for each class are significantly different at a 5 % level for each of the 5 parameters shown.

To find the parameters best suitable for surface classification we analyzed the difference between the waveform shapes coming from different surface types more quantitatively. We calculated the mean difference in the cumulative probability distributions for each parameter (Table 2). The difference between the distributions is much larger between leads and sea ice (0.72) than between the two evaluated sea ice types (0.52), making it much easier to detect leads within the ice than to distinguish between the two sea ice classes. Differences between the parameters are very small but they might be large enough to increase the rate of correct classification.

The largest difference between leads and sea ice can be found for the distribution of the power maximum and Leading and Trailing Edge Width. Since flat ice is the biggest challenge for the lead detection – flat ice results in a waveform similar to that obtained over leads – we analyzed the difference in the distributions from leads and flat first year ice (FYI3) more closely (right column in Table 2). We found the larger difference for the Maximum and Trailing Edge Width and selected these two parameters for lead detection within the ice.

Together with the Maximum and the TeW we found the TeS to be an adequate parameter to distinguish between MYI and FYI (Table 2). However, as the TeW and TeS are highly correlated, the TeS has been excluded from further analysis.

3.3 Detection of surface types

Results from the two classification methods based on Pulse Peakiness (PP), power maximum (Max) and Trailing Edge Width (TeW) are shown in Table 3. A simple threshold method based on the Pulse Peakiness is the approach used in the EnviSat processing chain (Ridout et al., 2012), therefore PP parameter has been included in the analysis for comparison. In Table 3 we don't show all possible parameter combinations but present only those leading to the best classification rates. Our classification rates are calculated as follows:

TCD
7, 1215–1242, 2013

The rates of correct classification for the different surface classes are the percentage of the waveforms coming from one class which have been correctly classified:

$$\text{correct classification}_{\text{class1}} = \frac{\#(\text{class}_{\text{class1}} \cap \text{known}_{\text{class1}})}{\#\text{known}_{\text{class1}}} \quad (2)$$

The rates of false detection are the percentage of waveforms classified as one class while actually belonging to another one:

$$\text{false classification}_{\text{class1}} = \frac{\#(\text{class}_{\text{class2}} \cap \text{known}_{\text{class1}})}{\#\text{class}_{\text{class2}}} \quad (3)$$

As we selected and divided our waveforms by random choice (for the threshold method we selected an equal number of waveforms of each class and for the Bayesian approach our data set has been divided into a learning and testing data set), each method has been performed 100 times. The presented classification rates are mean values and the standard deviation of our results did not exceed 2 %.

Based on the PP almost 95 % of the leads can be identified correctly (Table 3a. Based on the Max we found a lower averaged rate of correct classification of 87 % and a detection rate for leads around 83.8 %. The percentage of waveforms reflected from sea ice but falsely classified as lead however is strongly reduced for the Max parameter (6.5 %) compared to results obtained with the PP (12.6 %). Our Bayesian approach does not significantly increase the detection rate of leads, but decreases false classification for both leads and sea ice. The advantage of this method can also be shown by analyzing the critical case of flat first year ice (FYI3 in Fig. 5 and Table 1). For the basic threshold method based on the PP parameter more than 97 % of the waveforms coming from flat ice have been classified as leads, while for the Bayesian approach combining TeW and PP it is only 87 % (not shown in the Table).

Results for the two methods for the classification of FYI and MYI are shown in Table 3b. Here the use of the Bayesian method allows for a strong improvement of the classification by about 8 %, resulting in an average detection rate of almost 80 %. The

TCD
7, 1215–1242, 2013

rate of false classification can be lowered to about 10 % by using a combination of the TeW and Max. The simple threshold method results not only in a poor classification rate but also in a high rate of false classification, where 26 % of the waveform classified as FYI are actual MYI.

4 Discussion

The analysis of airborne radar altimeter data over arctic sea ice shows that the signals from first year ice and multi year ice differ significantly. A method to distinguish between these two ice types is presented based on waveform parameters Pulse Peakiness and the Trailing Edge Width. With a Bayesian based method we were able to classify around 80 % of the waveforms correctly. We can further confirm that a simple threshold method based on the Pulse Peakiness parameter is a sufficient method to detect leads. Adding more parameters or using a more advanced method as the Bayesian classifier does not significantly improve the rate of correct classification. Using Maximum instead of Pulse Peakiness can increase the accuracy in distinguishing leads from undeformed first year ice, but also reduce the detection rate of leads.

A related analysis has been performed by Drinkwater (1991) who analyzed data from a conventional pulse-limited radar altimeter in the marginal ice zone. He found similar results as obtained from our analysis: bare first year ice results in a high peak value of backscatter and a steep decay; rotten first year ice results in a lower backscatter and a lower decay gradient; and multi year ice results in a low peak and a low decay gradient. Despite these findings and even some clustering results that show a clear separation between FYI and MYI he was skeptical about the possibilities of sea ice classification. Fedor et al. (1988, 1989) also published sea ice classification results based on conventional airborne radar altimeter waveforms in the Beaufort Sea. He showed that the returned signal decreases from dark nilas over gray ice to more deformed ice types such as rough first year ice and multi year ice. Laxon (1994a) presented a method for sea ice classification based on the ERS data by parameterizing

TCD
7, 1215–1242, 2013

the waveform shape, but the method has only been used to distinguish between leads and sea ice. In the presented study the possibility to classify sea ice by waveform shape of beam-limited radar altimeters has been tested. In addition to a qualitative analysis, as done in previous studies, the presented classification method provides quantitative results. We show that the selected waveform parameters differ significantly for various surface classes and present a method where a combination of waveforms parameters leads to a correct classification of 80 % of the waveforms.

Numerous studies have been performed to understand the shape of the radar altimeter waveform and its sensitivity to surface conditions. Laboratory experiments have shown that as close to nadir the influence of electrical properties can be neglected (Beaven et al., 1995). The influence of surface roughness has been theoretically described by Brown (1977) and Raney (1998) and resulting challenges for the freeboard retrieval have been discussed by Hendricks et al. (2010). Based on the same laboratory experiments Beaven et al. (1995) also showed that the radar return originates at the snow/ice interface, and snow influence – as long as the snow is dry and cold – can be neglected. Dielectric properties of water however have been found to dominate over those of dry snow for volumetric water contents of 1 percent (Howell et al., 2005) which can occur at temperatures above −5 °C (Garrity, 1992). Based on forward modeling of the reflected radar signal, Makynen and Hallikainen (2009) found that this wet snow cannot be neglected and alters the waveform shape substantially by adding more volume scattering to the power echo. Willat et al. (2011) confirmed the influence of snow on the radar signal based on data from a dedicated field campaign. In the presented analysis the influence of surface roughness cannot be separated from the influence of snow properties. It can only be concluded that the combination of difference in ice and snow properties are sufficient to generate a significant difference in the waveform shape. More analysis is also required to test how our findings can be adapted to satellite borne altimeter systems. Both issues could be addressed in a large scale study of CryoSat-2 data combined with information about the surface roughness

TCD
7, 1215–1242, 2013

from, e.g. ASCAT scatterometer data (Andersen et al., 2007) and snow retrievals from passive microwave measurements.

As any other sea ice classification technique based on remote sensing the shown method might be limited to the central arctic in cold seasons (e.g. Kwok et al., 1992; Zakhvatkina, 2012; Kwok et al., 1992) where ice types are more distinct and a sufficient area of the radar footprint is covered by ice. The possibility to distinguish FYI from MYI by radar altimeter data alone is not intended to replace well-established large-scale classification methods based on scatterometer or passive microwave data (Fetterer et al., 1994; Fowler et al., 2004; Andersen et al., 2007; Maslanik et al., 2011; Polyakov et al., 2011). The main benefit of ice classification from radar altimeter data is for improvement of freeboard retrieval and thickness calculation. Freeboard, the part of the ice protruding from the water, is retrieved by detecting leads between the ice and finding the difference in elevation of ocean and ice floes. To retrieve the elevation a re-tracker needs to be applied to determine the position on the leading edge belonging to the surface. For the current ENVISAT algorithm different methods are applied for waveforms from sea ice and leads (Ridout et al., 2012). In our study we found the shape of the radar echo waveform to differ significantly between the first and multi year ice. Therefore we suggest that the recognition of different sea ice types can be used to develop a more accurate re-tracker. More work, however, is required to test this possibility. The calculation of sea ice thickness from the freeboard measurements is based on the assumption of hydrostatic equilibrium

$$h_i = \frac{f_i \rho_w}{\rho_w - \rho_i} + \frac{h_s \rho_s}{\rho_w - \rho_i} \quad (4)$$

where f_i is the ice freeboard, ρ_i the ice density, ρ_w the density of water ρ_s, density of snow and h_s the snow load. The highest uncertainties come from the freeboard retrieval itself, the snow load and to some extent from the density of the ice (Forström et al., 2011; Alexandrov et al., 2010). So far snow load has been taken from climatologies (Warren et al., 1999) which are based on measurements on multi year ice. Recent

TCD
7, 1215–1242, 2013

results from IceBridge laser data over arctic sea ice however reveal a significant smaller snow load on first year ice compared to multi year ice where the snow accumulates over the entire season (Kurtz and Farrell, 2011). The presented method therefore allows not only to improve the freeboard retrieval but allows to use ice type dependent values for the sea ice density and snow load.

5 Conclusions

It was found that the signals retrieved over first year ice and multi year differ significantly. Various parameters to describe the shape of the radar echo waveform from different sea ice types were analyzed. The Maximum of the returned power echo and the Trailing Edge Width were selected as the most suitable ones for sea ice classification. A Bayesian approach used in combination with the waveform parameters was found to be more suitable to distinguish between the two ice types. With these methods it was possible to detect 80 % of the waveforms correctly. In addition a simple threshold method based on the widely used Pulse Peakiness was used for lead detection. It was shown that use of the Maximum parameter could lower the rate of false detection of leads. More analysis is required to test the presented method for satellite based altimeters. The method has potential to improve the freeboard retrieval by developing a more accurate re-tracker algorithm and improve the conversion into sea ice thickness by applying surface dependent values for sea ice density and snow load.

Acknowledgements. This work is supported by the Research Council of Norway through the ROMFORSK programme (project no. 202313/V30) and ESA PRODEX contract no 4200090318 CN1. We thank the CryoVEx teams from the Alfred Wegener Institute and the Danish National Space Institute, Danish Technical University (DTU Space) for their work during the campaigns and the data processing. We gratefully acknowledge the comments from Kjell Kloster and Natalia Ivanova on our manuscript. The shown SAR image from 1 May is obtained from the European Space Agency.

TCD
7, 1215–1242, 2013

References

Alexandrov, V., Sandven, S., Wahlin, J., and Johannessen, O. M.: The relation between sea ice thickness and freeboard in the Arctic, The Cryosphere, 4, 373–380, doi:10.5194/tc-4-373-2010, 2010. 1228

Andersen, S., Breivik, L., Eastwood, S., Godøy, Ø., Lind, M., Porcires, M., and Schyberg, H.: OSI SAF Sea Ice Product Manual–v3. 5, EUMETSAT OSI SAF–Ocean and Sea Ice Sattelite Application Facility, Tech. Rep. SAF/OSI/met. no/TEC/MA/125, 2007. 1228

Bayes, T. and Price, M.: An Essay Towards Solving a Problem in the Doctrine of Chances, By the Late Rev. Mr. Bayes, FRS communicated by Mr. Price, in a letter to John Canton, AMFRS, Philosophical Transactions (1683–1775), 370–418, 1763. 1222

Beaven, S., Lockhart, G., Gogineni, S., Hossetnmostafa, A., Jezek, K., Gow, A., Perovich, D., Fung, A., and Tjuatja, S.: Laboratory measurements of radar backscatter from bare and snow-covered saline ice sheets, Int. J. Remote Sens., 16, 851–876, 1995. 1227

Brown, G.: The average impulse response of a rough surface and its applications, IEEE T. Antenn. Propag., 25, 67–74, 1977. 1218, 1227

Chase, J. and Holyer, R.: Estimation of sea ice type and concentration by linear unmixing of Geosat altimeter waveforms, J. Geophys. Res., 95, 18015–18018, 1990. 1217

Comiso, J. C., Parkinson, C. L., Gersten, R., and Stock, L.: Accelerated decline in the Arctic sea ice cover, Geophys. Res. Lett., 34, L01703, doi:10.1029/2007GL031972, 2007. 1216

Cullen, R. and Davidson, M.: Arctic experiments to support CryoSat-2 validation, in: EGU General Assembly Conference Abstracts, vol. 11, 10588 pp., 2009. 1219

Drinkwater, M.: Ku band airborne radar altimeter observations of marginal sea ice during the 1984 marginal ice zone experiment, J. Geophys. Res., 96, 4555–4572, 1991. 1217, 1226

Drinkwater, M., Francis, R., Ratier, G., and Wingham, D.: The European Space Agency's earth explorer mission CryoSat: measuring variability in the cryosphere, Ann. Glaciol., 39, 313–320, 2004. 1217

Dwyer, R. and Godin, R.: Determining sea-ice boundaries and ice roughness using GEOS-3 altimeter data, 1980. 1217

Fedor, L., Hayne, G., and Walsh, E.: Airborne pulse-limited radar altimeter return waveform characteristics over ice in the Beaufort Sea, in: OCEANS'88: a Partnership of Marine Interests, Proceedings, IEEE, 1704–1710, 1988. 1226

TCD
7, 1215–1242, 2013

Fedor, L., Hayne, G., and Walsh, E.: Ice-type Classifications From Airborne Pulse-limited Radar Altimeter Return Waveform Characteristics, in: Geoscience and Remote Sensing Symposium, 1989, IGARSS'89, 12th Canadian Symposium on Remote Sensing, 1989 International, vol. 3, 1949–1952, IEEE, 1989. 1226

Fetterer, F.: Sea ice altimetry, Tech. rep., DTIC Document, 1992. 1217

Fetterer, F., Gineris, D., and Kwok, R.: Sea ice type maps from Alaska synthetic aperture radar facility imagery: an assessment, J. Geophys. Res., 99, 22–22, 1994. 1228

Forström, S., Gerland, S., and Pedersen, C.: Thickness and density of snow-covered sea ice and hydrostatic equilibrium assumption from in situ measurements in Fram Strait, the Barents Sea and the Svalbard coast, Ann. Glaciol., 52, 261–271, 2011. 1228

Fowler, C., Emery, W., and Maslanik, J.: Satellite-derived evolution of Arctic sea ice age: October 1978 to March 2003, IEEE Geosci. Remote S., 1, 71–74, 2004. 1228

Garrity, C.: Characterization of snow on floating ice and case studies of brightness temperature changes during the onset of melt, Geoph. Monog. Series, 68, 313–328, 1992. 1227

Giles, K., Laxon, S., Wingham, D., Wallis, D., Krabill, W., Leuschen, C., McAdoo, D., Manizade, S., and Raney, R.: Combined airborne laser and radar altimeter measurements over the Fram Strait in May 2002, Remote Sens. Environ., 111, 182–194, 2007. 1217, 1221

Giles, K., Laxon, S., and Ridout, A.: Circumpolar thinning of Arctic sea ice following the 2007 record ice extent minimum, Geophys. Res. Lett., 35, L22502, doi:10.1029/2008GL035710, 2008. 1216, 1217

Haas, C., Gerland, S., Eicken, H., and Miller, H.: Comparison of sea-ice thickness measurements under summer and winter conditions in the Arctic using a small electromagnetic induction device, Geophysics, 62, 749–757, 1997. 1216

Haas, C., Hendricks, S., Eicken, H., and Herber, A.: Synoptic airborne thickness surveys reveal state of Arctic sea ice cover, Geophys. Res. Lett., 37, doi:10.1029/2010GL042652, 2010. 1216

Haas, C., Goff, H., Audrain, S., Perovich, D., and Haapala, J.: Comparison of seasonal sea-ice thickness change in the Transpolar Drift observed by local ice mass-balance observations and floe-scale EM surveys, Ann. Glaciol., 52, 97–102, 2011. 1216

Helm, V. and Steinhage, D.: CryoVEx 2007-Data Acquisition and Final Processing Report, Tech. rep., 2008. 1219

TCD
7, 1215–1242, 2013

Hendricks, S., Stenseng, L., Helm, V., and Haas, C.: Effects of surface roughness on sea ice freeboard retrieval with an Airborne Ku-Band SAR radar altimeter, in: Geoscience and Remote Sensing Symposium (IGARSS), 2010 IEEE International, 3126–3129, 2010. 1227

Hendricks, S., Gerland, S., Smedsrud, L., Haas, C., Pfaffhuber, A., and Nilsen, F.: Sea-ice thickness variability in Storfjorden, Svalbard, Ann. Glaciol., 52, 61–68, 2011. 1216

Howell, S., Yackel, J., De Abreu, R., Geldsetzer, T., and Breneman, C.: On the utility of SeaWinds/QuikSCAT data for the estimation of the thermodynamic state of first-year sea ice, IEEE T. Geosci. Remote, 43, 1338–1350, 2005. 1227

Hvidegaard, S. M., Forsberg, R., Helm, V., Hendricks, S., Skourup, H., Stenseng, L., Hanson, S., and Haas, C.: CryoVEx 2008 Final Report, Tech. rep., Dansh National Space Institute, DTU Space, 2009. 1219

Kurtz, N. and Farrell, S.: Large-scale surveys of snow depth on Arctic sea ice from operation IceBridge, Geophys. Res. Lett., 38, L20505, doi:10.1029/2011GL049216, 2011. 1229

Kwok, R.: The RADARSAT geophysical processor system, 1996.

Kwok, R.: Sea ice concentration estimates from satellite passive microwave radiometry and openings from SAR ice motion, Geophys. Res. Let., 29, 25-1–25-4, 2002. 1216

Kwok, R. and Rothrock, D.: Decline in Arctic sea ice thickness from submarine and ICESat records: 1958–2008, Geophys. Res. Lett., 36, L15501, doi:10.1029/2009GL039035, 2009. 1216

Kwok, R. and Untersteiner, N.: The thinning of Arctic sea ice, Phys. Today, 64, 36–41, 2011. 1217

Kwok, R., Rignot, E., Holt, B., and Onstott, R.: Identification of sea ice types in spaceborne synthetic aperture radar data, J. Geophys. Res., 97, 2391–2402, 1992. 1228

Kwok, R., Zwally, H., and Yi, D.: ICESat observations of Arctic sea ice: a first look, Geophys. Res. Lett, 31, L16401, doi:10.1029/2004GL020309, 2004. 1217

Laxon, S.: Sea ice altimeter processing scheme at the EODC, Int. J. Remote Sens., 15, 915–924, 1994a. 1217, 1226

Laxon, S.: Sea ice extent mapping using the ERS-1 radar altimeter, EARSeL Advances in Remote Sensing, 3, 112–116, 1994b. 1220

Laxon, S., Peacock, N., and Smith, D.: High interannual variability of sea ice thickness in the Arctic region, Nature, 425, 947–950, 2003. 1216, 1217

TCD
7, 1215–1242, 2013

Legresy, B., Papa, F., Remy, F., Vinay, G., van den Bosch, M., and Zanife, O.: ENVISAT radar altimeter measurements over continental surfaces and ice caps using the ICE-2 retracking algorithm, Remote Sens. Environ., 95, 150–163, 2005. 1220

Makynen, M. and Hallikainen, M.: Simulation of ASIRAS altimeter echoes for snow-covered first-year sea ice, IEEE Geosci. Remote S., 6, 486–490, 2009. 1227

Maslanik, J., Fowler, C., Stroeve, J., Drobot, S., Zwally, J., Yi, D., and Emery, W.: A younger, thinner Arctic ice cover: Increased potential for rapid, extensive sea-ice loss, Geophys. Res. Lett., 34, L24501, doi:10.1029/2007GL032043, 2007. 1216

Maslanik, J., Stroeve, J., Fowler, C., and Emery, W.: Distribution and trends in Arctic sea ice age through spring 2011, Geophys. Res. Lett., 38, L13502, doi:10.1029/2011GL047735, 2011. 1228

Onstott, R., Grenfell, T., Matzler, C., Luther, C., and Svendsen, E.: Evolution of microwave sea ice signatures during early summer and midsummer in the marginal ice zone, J. Geophys. Res., 92, 6825–6835, 1987. 1217

Peacock, N. and Laxon, S.: Sea surface height determination in the Arctic Ocean from ERS altimetry, J. Geophys. Res, 109, C07001, doi:10.1029/2001JC001026, 2004. 1217, 1221

Polyakov, I., Kwok, R., and Walsh, J.: Recent changes of arctic multiyear sea-ice coverage and the likely causes, B. Am. Meteorol. Soc., 92, 145–151, doi:10.1175/BAMS-D-11-00070.1, 2011. 1228

Raney, R.: The delay/Doppler radar altimeter, IEEE T. Geosci. Remote, 36, 1578–1588, 1998. 1218, 1227

Ridout, A., Ivanova, N., Tonboe, R., Laxon, S., Timms, G., and Kern, S. Kloster, K.: Algorithm Theoretical Basis Document SICCI-ATBDv0-07-12 Version 1.1./03Sept 2012, Tech. rep., ESA, 2012. 1217, 1224, 1228

Röhrs, J. and Kaleschke, L.: An algorithm to detect sea ice leads by using AMSR-E passive microwave imagery, The Cryosphere, 6, 343–352, doi:10.5194/tc-6-343-2012, 2012. 1221

Rothrock, D., Yu, Y., and Maykut, G.: Thinning of the Arctic sea-ice cover, Geophys. Res. Lett., 26, 3469–3472, 1999. 1216

Rothrock, D., Percival, D., and Wensnahan, M.: The decline in arctic sea-ice thickness: Separating the spatial, annual, and interannual variability in a quarter century of submarine data, J. Geophys. Res., 113, C05003, doi:10.1029/2007JC004252, 2008. 1216

Stroeve, J., Serreze, M., Holland, M., Kay, J., Malanik, J., and Barrett, A.: The Arctic's rapidly shrinking sea ice cover: a research synthesis, Climatic Change, 1–23, 2012. 1216

TCD
7, 1215–1242, 2013

Ulander, L.: Interpretation of Seasat radar-altimeter data over sea ice using near-simultaneous SAR imagery, Int. J. Remote Sens., 8, 1679–1686, 1987. 1217
Warren, S., Rigor, I., Untersteiner, N., Radionov, V., Bryazgin, N., Aleksandrov, Y., and Colony, R.: Snow depth on Arctic sea ice, J. Climate, 12, 1814–1829, 1999. 1217, 1228
Willat, R., Laxon, S., Giles, K.and Cullen, R., Haas, C., and Helm, V.: Ku-band radar penetration into snow cover on Arctic sea ice using airborne data, Ann. Glaciol., 52, 197–205, 2011. 1227
Zakhvatkina, N.: Classification of Sea Ice Types in ENVISAT Synthetic Aperture Radar Images, IEEE ASSP Magazine, 2012. 1228

TCD
7, 1215–1242, 2013

Table 1. Overview of the study areas and the numbers of available echo waveforms at each case. We evaluated nine cases: two for leads (L), four for first year ice (FYI) and three for multi year ice (MYI) each containing several hundred of waveforms. Additional data sets which have been used for obtaining information about the surface type are listed in the right column. ASAR indicates that an ESA EnviSat ASAR image was available.

Cases	Date	Description	nr of echos	additional data sets
L 1	27.04.2008	Leads north east of Greenland	566	ASAR, Photo Camera
L 2	01.05.2008	Leads north of Alert	1635	ASAR, Photo Camera
FYI 1	21.04.2007	Svalbard Walenbergfjorden, fast ice	3273	ASAR
FYI 2	06.05.2008	Baffin Bay	10755	ASAR
FYI 3	01.05.2008	Thin, flat, snow covered ice north of Alert	5248	ASAR, in-situ, EM-Bird, Photo Camera
FYI 4	01.05.2008	Validation area North of Alert	513	ASAR, Photo Camera
MYI 1	27.04.2008	Big ice field north east of Greenland	7223	ASAR, Photo Camera
MYI 2	01.05.2008	Sea ice field north of Alert	7205	ASAR, Photo Camera
MYI 3	01.05.2008	Validation area North of Alert	796	ASAR, in-situ, EM-Bird, Photo Camera

TCD
7, 1215–1242, 2013

Table 2. Mean distances between the empirical cumulative distribution functions of the five parameters determined from KS-test: pulse peakiness (PP), trailing edge slope (TeS), leading edge width (LeW), trailing edge width (TeW), and the power maximum (Max).

	leads vs sea ice	FYI vs MYI	leads vs flat FYI
PP	0.718	0.518	0.236
TeS	0.716	0.523	0.250
LeW	0.721	0.511	0.251
TeW	0.720	0.527	0.269
Max	0.737	0.521	0.307

TCD
7, 1215–1242, 2013

Table 3. Results for the two different classification methods: rule based threshold and Bayesian classifier. The overall classification rates, the probabilities of correct and false detection for ice and leads (left) and for first year ice and multi year ice (right) are presented. The classification rates are defined in Eqs. (2) and (3). The used parameters are the pulse peakiness (PP), the power maximum (Max) and the trailing edge width (TeW).

Method	Threshold		Bayes	Method	Threshold	Bayes	
Parameter	PP	Max	TeW and max	Parameter	PP	TeW and Max	TeW and PP
Correct classifications [%]				Correct classifications [%]			
all	88.0	87.3	91.3	all	72.4	80.3	79.9
Leads	94.2	83.8	94.9	FYI	72.6	78.7	80.5
Ice	79.5	90.8	89.1	MYI	68.6	81.7	75.5
False classifications [%]				False classifications [%]			
Leads	12.6	6.5	6.2	FYI	26.0	10.4	23.7
Ice	5.6	12.0	2.3	MYI	19.2	9.1	15.7
not classified	4.6	3.7	6.9	not classified	6.2	11.3	12.8

TCD
7, 1215–1242, 2013

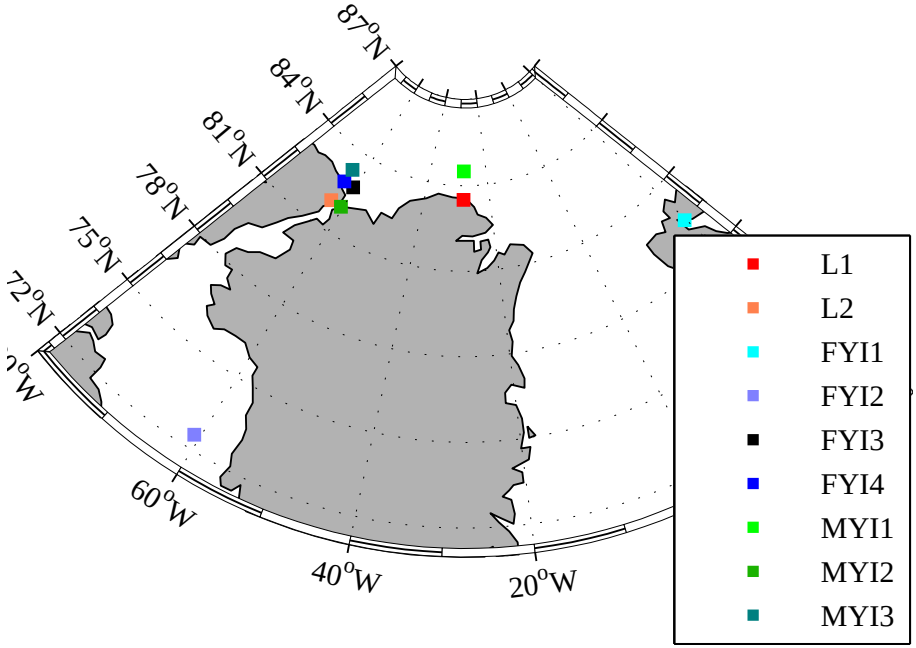

Fig. 1. Map showing the approximate location for each of the evaluated cases (see detailed description in Table 1). cases with Leads (L) are marked in red colors, first year ice (FYI) in blue and multi year ice (MYI) in green.

TCD
7, 1215–1242, 2013

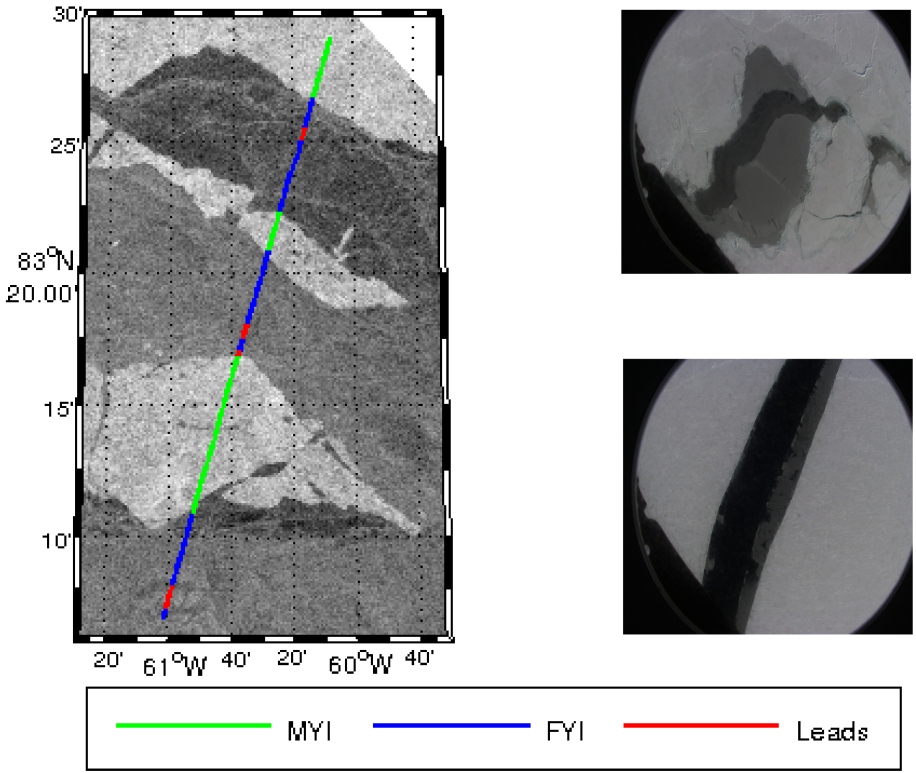

Fig. 2. Left: ASIRAS track from the 1 May 2008 overlaid on a contemporary ESA Envisat ASAR image. The image has been used for obtaining information about the real sea ice type for validation of our algorithm. In green the ASIRAS track over MYI is shown, in blue FYI and in red the leads. Right: example of camera images used additionally for identifying the leads within the ice.

TCD
7, 1215–1242, 2013

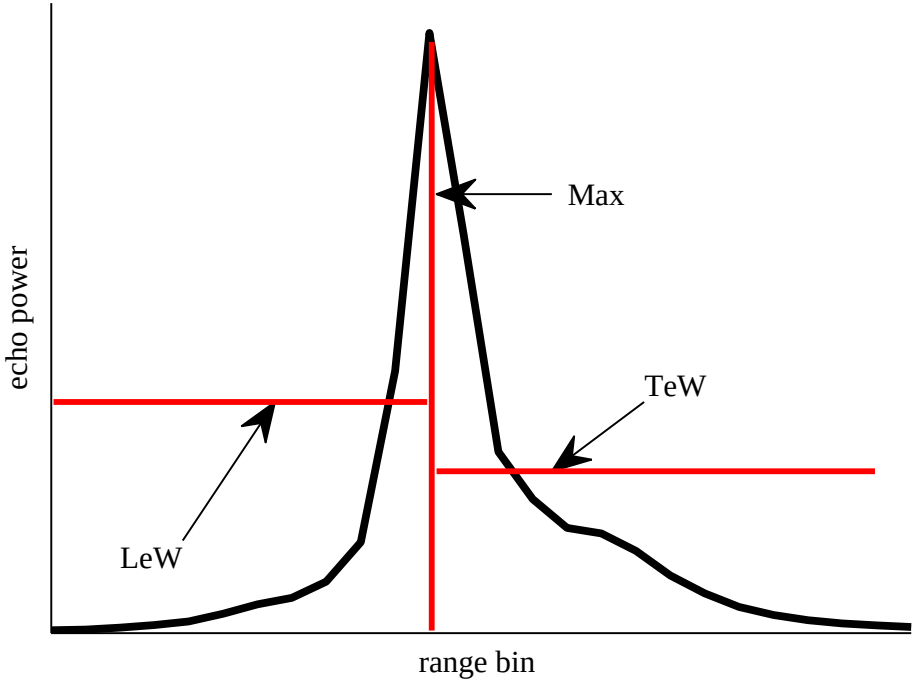

Fig. 3. Visualization of waveform parameters. Here a subset of the averaged waveform for first year ice is shown. The leading edge width (LeW) ist based on a gaussian fit and the trailing edge width (TeW) on exponential decay function.

TCD
7, 1215–1242, 2013

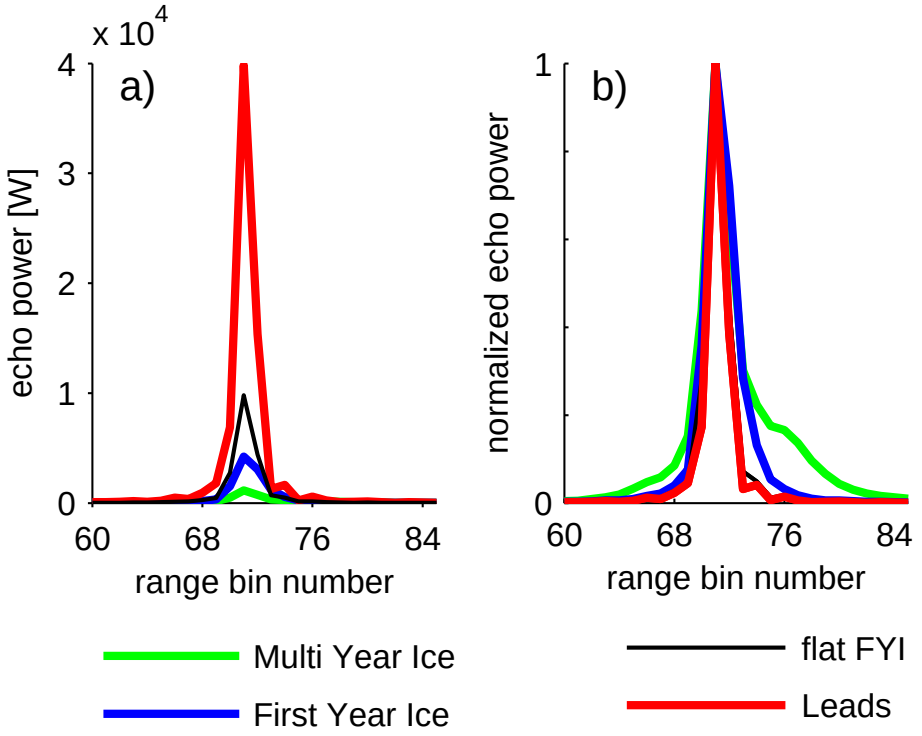

Fig. 4. Averaged waveforms for the three evaluated surface types: leads (red), first year ice (blue) and multi year ice (green). Additionally the mean signal over flat FYI is shown (black). The waveform have been calculated as a mean of all available measurements for these surface type. **(a)** Mean reflected power waveform for each surface type.**(b)** Normalized mean waveform to show the difference in the width of the reflected signal.

TCD
7, 1215–1242, 2013

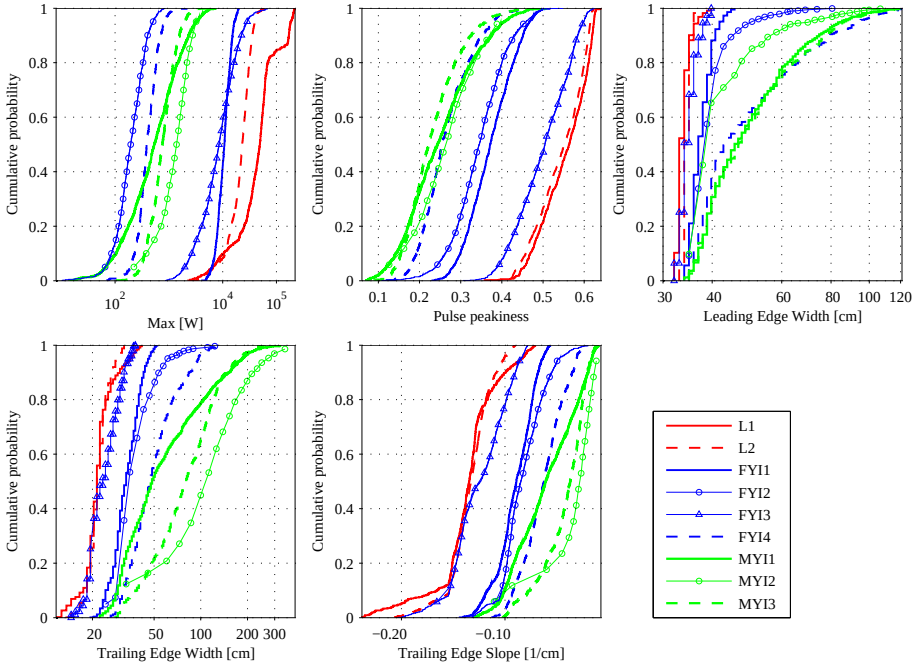

Fig. 5. Cumulative probability distributions for the nine cases (see Table 1) for the five waveform parameters: Max, pulse peakiness, leading edge width, trailing edge width and trailing edge slope. Distributions obtained from waveforms resulting from leads are shown in red, from first year ice in blue and multi year ice in green.

TCD
7, 1215–1242, 2013